International Journal of Heat and Mass Transfer 127 (2018) 7–15

Contents lists available at ScienceDirect

International Journal of Heat and Mass Transfer

journal homepage: www.elsevier.com/locate/ijhmt

Numerical investigation of blunt body's heating load reduction with combination of spike and opposing jet

Feng Qu [a], Di Sun [a], Junqiang Bai [a,*], Guang Zuo [b], Chao Yan [c]

[a] School of Aeronautics, Northwestern Polytechnical University, Xi'an 710072, China
[b] Institute of Manned Space System Engineering, China Academy of Space Technology, Beijing 100094, China
[c] National Laboratory for CFD, Beihang University, Beijing 100191, China

ARTICLE INFO

Article history:
Received 29 March 2018
Received in revised form 8 June 2018
Accepted 29 June 2018

Keywords:
Computational fluid dynamics
Nozzle
Hypersonic heating
Jet
Re-entry vehicle

ABSTRACT

In the design of the new generation reusable re-entry space vehicle, how to effectively reduce the heating load is important. In this paper, the thermal protection system combining the spike technology with the opposing jet technology is investigated. The three-dimensional compressible Reynolds Averaged Navier–Stokes (RANS) equations are simulated and Menter's shear stress transport (SST) turbulence model is applied. Also, the all-speed flux scheme called E-AUSMPWAS is adopted. The grid study is done and the numerical procedure is validated. Models with spikes of different lengths and opposing jets of different pressures are compared. Results show that the total pressure of the jet and the length of the spike have significant influences on the peak heating load of the vehicle. Also, the total heating load can reduce almost 95% compared to the base model. The findings suggest that the thermal protection system, which combines the spike technology with the opposing jet technology, is promising to be widely used in the design of the new generation reusable re-entry space vehicle.

1. Introduction

Nowadays, the new generation reusable re-entry space vehicle which is capable of carrying out deep space exploration has got wide attention. However, the structural coefficients of the existing spacecraft, such as Shen Zhou manned spacecraft and Apollo manned spaceship, are so large as to make payload not enough to achieve this goal [1]. Therefore, it is necessary to adopt more reusable lightweight materials and large-scale thin-wall structures to replace the tradition thermal protection method. Because the severe heating load is crucial to the design and optimization of the thermal protection system, how to effectively reduce the vehicle's heating load is of great significance [2].

In general, various techniques have been studied to achieve the heating load's reduction, such as spike [3–9], energy deposition [10], opposing jet [11–13], and their combinations [14–20]. As illustrated in Fig. 1, the spike technology splits the bow shock into multiple weaker shock waves and induces a large flow separation zone in the vicinity of the stagnation region. Therefore, it is capable of reducing the heating load by reconstructing the flow field. However, the heating load at the head of the spike is severe. Also, the shock/shock interaction and the reattachment of the separation zone at the shoulder make the peak heat flux high.

The opposing jet pushes the shock away from the stagnation region and forms a series of rich flow structures. Due to its wide application, a large number of studies have been carried out on this issue. Finely pointed out that the flow field induced by the opposing jet had the following three modes: the unsteady modes of the shock with oscillations, the steady modes of the shock without oscillations, and the medium mode between them [21]. Tian studied the influences of the jet Mach number, the angle of attack, and the free Mach number on the heating load's reduction by adopting numerical methods [22]. Hayashi carried out numerical simulations and experiments to study the opposing jet's method with his co-workers [23]. Also, Huang conducted similar analyses and obtained constructive conclusions [24]. However, the jet has to be with a large total pressure to form a stable flow field, which limits this method's wide use.

To overcome the defects of the spike technology and the opposing jet technology, several combinatorial strategies were proposed. Among them, the thermal protection system by combining the spike technology with the opposing jet technology have been pursued by numerous scholars [25]. Experiments carried out by Liu and Jiang showed that the peak heating load was reduced remarkably by this combinatorial technology [26]. Huang numerically studied the technology's performance in reducing drag [27]. Based

* Corresponding author.
E-mail address: junqiang@nwpu.edu.cn (J. Bai).

https://doi.org/10.1016/j.ijheatmasstransfer.2018.06.154
0017-9310/

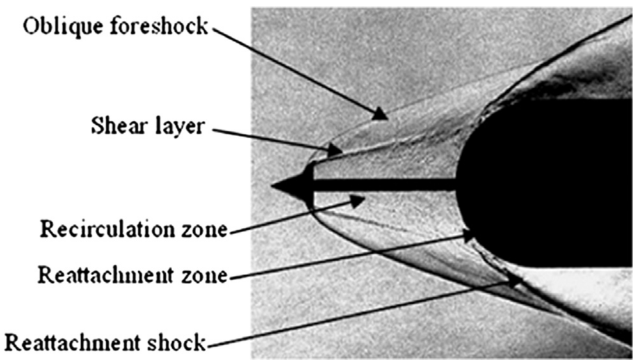

Fig. 1. Flowfield induced by the spike [5].

on high precision numerical approach, Eghlima et al. found that the combinatorial technology could reduce the peak heating load greatly [20]. However, they only consider the peak heating load and ignore the total heating load. In fact, the total heating load is of much significance to the design of the thermal protection system.

In this paper, we will adopt numerical methods to study the influence of the thermal protection system, which combines the opposing jet technology with the spike technology, on both the peak heating load and the total heating load. Moreover, spikes with different lengths and jets with different total pressures are considered.

This manuscript is organized as follows. In the second section, we will briefly overview the governing equations and the computational methods we adopt. Validation for the code and numerical procedure, and the grid category are carried out in Secttion 3. The fourth section will illustrate the physical models which we analyze in this paper. Results and discussions will be presented in the 5th section. The last section contains the concluding remarks.

2. Governing equations and numerical procedure

2.1. Governing equations

In this study, we adopt the following three-dimensional steady NS equations to numerically solve the flow fields [28,29].

Continuity equation:

$$\frac{\partial \rho}{\partial t} + \frac{\partial \rho u_i}{\partial x_i} = 0 \tag{1}$$

Momentum equation:

$$\frac{\partial(\rho u_i)}{\partial t} + \frac{\partial(\rho u_i u_j)}{\partial x_j} = -\frac{\partial p}{\partial x_i} + \frac{\partial \tau_{ij}}{\partial x_j} \tag{2}$$

Energy equation:

$$\frac{\partial(\rho E)}{\partial t} + \frac{\partial(\rho u_j H)}{\partial x_j} = \frac{\partial(u_i \tau_{ij} - \dot{q}_j)}{\partial x_j} \tag{3}$$

where ρ is the density, u_i is the i^{th} component velocity. Also, p is the static pressure, τ_{ij} is the shear stress term, $\dot{q}_j$ is the heat flux, E is the total energy, and H is the total enthalpy as follows

$$p = (\gamma - 1)\left[\rho E - \frac{1}{2}\rho(u^2 + v^2 + w^2)\right] \tag{4}$$

$$E = e + \frac{1}{2}(u^2 + v^2 + w^2) \tag{5}$$

$$H = e + \frac{p}{\rho} \tag{6}$$

$$\begin{aligned}
\tau_{xx} &= \frac{2}{3}\mu\left(2\frac{\partial u}{\partial x} - \frac{\partial v}{\partial y} - \frac{\partial w}{\partial z}\right); \quad \tau_{xy} = \tau_{yx} = \mu\left(\frac{\partial u}{\partial y} + \frac{\partial v}{\partial x}\right) \\
\tau_{yy} &= \frac{2}{3}\mu\left(2\frac{\partial v}{\partial y} - \frac{\partial u}{\partial x} - \frac{\partial w}{\partial z}\right); \quad \tau_{yz} = \tau_{zy} = \mu\left(\frac{\partial v}{\partial z} + \frac{\partial w}{\partial y}\right) \\
\tau_{zz} &= \frac{2}{3}\mu\left(2\frac{\partial w}{\partial z} - \frac{\partial u}{\partial x} - \frac{\partial v}{\partial y}\right); \quad \tau_{zx} = \tau_{xz} = \mu\left(\frac{\partial w}{\partial x} + \frac{\partial u}{\partial z}\right)
\end{aligned} \tag{7}$$

$$\begin{aligned}
q_x &= -\frac{\mu}{(\gamma - 1)Pr}\frac{\partial T}{\partial x} \\
q_y &= -\frac{\mu}{(\gamma - 1)Pr}\frac{\partial T}{\partial y} \\
q_z &= -\frac{\mu}{(\gamma - 1)Pr}\frac{\partial T}{\partial z}
\end{aligned} \tag{8}$$

Herein, u, v, w denote the velocity in Cartesian coordinates, T is the static temperature, e is the internal energy, and γ denotes the specific heat ratio.

2.2. Turbulence model

In this paper, we adopt the RANS eddy-viscosity model in which the shear stress term is the sum of a laminar and a turbulent component. That is to say, the RANS equations are equivalent to the NS equations in Eq. (1) with the exception that μ is replaced by $\mu + \mu_T$ in Eq. (7) and μ/Pr is replaced by $\mu/Pr + \mu_T/Pr_T$ in Eq. (8), where $Pr = 0.72$, $Pr_T = 0.9$, and μ_T is the eddy viscosity [30,31].

Among the existing RANS models, the SST turbulence model developed by Menter combines the merits of the original k-ω model and the standard k-ε model [32]. It has been widely used due to its high efficiency and robustness. The model can be written as follows:

$$\frac{\partial(\rho k)}{\partial t} + \frac{\partial(\rho u_j k)}{\partial x_j} = \frac{\partial}{\partial x_j}\left[(\mu_L + \sigma_k \mu_T)\frac{\partial k}{\partial x_j}\right] + P_k - \beta^* \rho \omega k \tag{9}$$

$$\begin{aligned}
\frac{\partial(\rho \omega)}{\partial t} + \frac{\partial(\rho u_j \omega)}{\partial x_j} &= \frac{\partial}{\partial x_j}\left[(\mu_L + \sigma_\omega \mu_T)\frac{\partial \omega}{\partial x_j}\right] + P_\omega - \beta \rho \omega^2 \\
&\quad + 2(1 - f_1)\frac{\rho \sigma_{\omega 2}}{\omega}\frac{\partial k}{\partial x_j}\frac{\partial \omega}{\partial x_j}
\end{aligned} \tag{10}$$

where k denotes the turbulent kinetic energy, ω is the turbulent dissipation rate, P_k and P_ω denote the production terms of the term k and the term ω, μ_L is the laminar viscosity, and μ_T denotes the turbulent viscosity.

The P_k and P_ω can be obtained by

$$P_k = \mu_T \Omega^2, P_\omega = C_\omega \rho \Omega^2$$

where Ω is the magnitude of the vorticity.

The eddy viscosity is set as

$$\mu_T = \frac{a_1 \rho K}{\max(a_1 \omega, f_2 \|\Omega\|)}$$

$$\phi = f_1 \phi_1 + (1 - f_1)\phi_2 \quad f_1 = \tanh(\Gamma_1^4)$$

$$\begin{aligned}
\Gamma_1 &= \min\left[\max\left(\frac{\sqrt{K}}{0.09\omega d}, \frac{500\mu_L}{\rho \omega d^2}\right), \frac{4\rho \sigma_{\omega 2} K}{CD_{K\omega} d^2}\right] \quad CD_{K\omega} \\
&= \max\left(2\frac{\rho \sigma_{\omega 2}}{\omega}\frac{\partial K}{\partial x_j}\frac{\partial \omega}{\partial x_j}, 1 \times 10^{-20}\right)
\end{aligned}$$

where d is the distance to the nearest wall. The f_2 term is given by:

$$f_2 = \tanh(\Gamma_2^4) \quad \Gamma_2 = \max\left(\frac{2\sqrt{K}}{0.09\omega d}, \frac{500\mu_L}{\rho \omega d^2}\right)$$